Role of Defects and Growth Directions in the Formation of Periodically Twinned and Kinked Unseeded Germanium Nanowires

ARTICLE *in* CRYSTAL GROWTH & DESIGN · APRIL 2011

Impact Factor: 4.89

7 AUTHORS, INCLUDING:

Christopher A Barrett
University of Georgia
14 PUBLICATIONS **247** CITATIONS

CRYSTAL GROWTH & DESIGN

ARTICLE

pubs.acs.org/crystal

Role of Defects and Growth Directions in the Formation of Periodically Twinned and Kinked Unseeded Germanium Nanowires

Hugh Geaney,[†] Calum Dickinson,[†] Weihao Weng,[‡] Christopher J. Kiely,[‡] Christopher A. Barrett,[†] Robert D. Gunning,[†,#] and Kevin M. Ryan[*,†,#]

[†]Materials and Surface Science Institute and Department of Chemical and Environmental Sciences, University of Limerick, Limerick, Ireland

[‡]Department of Materials Science and Engineering, Lehigh University, Bethlehem, Pennsylvania 18015-3195, United States

[#]SFI-Strategic Research Cluster in Solar Energy Research, University of Limerick, Limerick, Ireland

Supporting Information

ABSTRACT: Here we show the impact of preferred growth directions and defects in the formation of complex Ge nanowire (NW) structures grown by a simple organic medium based synthesis. Various types of NWs are examined including: straight defect free NWs; periodically bent NWs with precise angles between the NW segments; NWs with mutually exclusive lateral or longitudinal faults; and more complex "wormlike" structures. We show that choice of solvent and reaction temperature can be used to tune the morphology of the NWs formed. The various types of NWs were probed in depth using transmission electron microscopy (TEM), scanning electron microscopy (SEM), selected area electron diffraction (SAED), and dark field TEM (DFTEM).

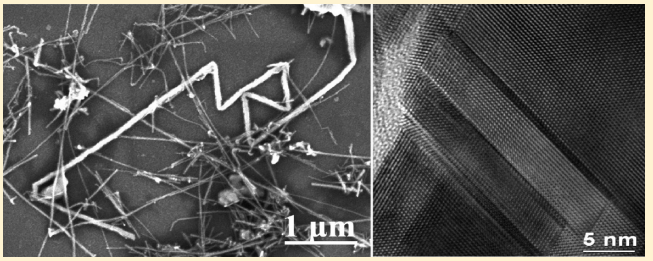

I. INTRODUCTION

The unique size-dependent properties associated with one-dimensional (1D) Ge nanostructures have generated a wave of synthetic research based on Ge nanowire (NW) growth. Specifically, they are of interest due to their potential as anode and charge carrier paths in lithium ion batteries, use in photoresistors, and suitability for next generation solar cells.[1−6] Furthermore, a renewed interest in the utilization of Ge has emerged in the semiconductor industry due to the successful introduction of hafnium oxide as a dielectric lowering the encumbrance to non-silicon material integration.[7] Notably, crystalline Ge possesses greater intrinsic carrier mobility and a larger Bohr excitonic radius than Si, making it a more promising candidate material for NW based metal-oxide-semiconductor field-effect transistor (MOSFET) technology.[8,9]

Synthetic methods for the preparation of Ge nanowires are varied and include such techniques as laser ablation, molecular beam epitaxy, chemical vapor deposition (CVD), and a variety of different solution based processes.[10−13] These methods are catalytic in nature requiring a metal nanoparticle seed with NW growth occurring by the well established vapor−liquid−solid (VLS)[14,15] and vapor−solid−solid (VSS)[16,17] protocols. An alternative strategy for Ge NW growth is the metal catalyst free, high boiling point solvent (HBS) based approach.[18−20] Recently, we have developed a method which facilitates the growth of high yields of crystalline wires directly on substrates within the vapor phase of the HBS.[21] The growth morphology of NWs produced by unseeded approaches is less understood than their seeded analogues, representing a barrier to broad application.

A wide variety of growth morphologies have been noted in metal seeded NWs. Factors such as NW growth direction and kinking are important when tailoring NWs for applications ranging from transistors to sensors.[22,23] The growth direction for Si and Ge NWs has been widely studied and modulated.[24−26] Typically, VLS grown group IV NWs exhibit ⟨111⟩ growth directions, while growth in ⟨110⟩, ⟨100⟩, and ⟨112⟩ directions has also been observed.[24,27,28] Careful control over the growth orientation is particularly important when epitaxial growth from crystalline substrates is desired.[29,30] Structural variations within NWs, such as lamellar twinning faults, have been noted in a number of seeded approaches and must be understood and controlled as they can impact the electrical and optical properties of the NWs.[31] Faults parallel and perpendicular to either the ⟨111⟩ or ⟨112⟩ growth direction of Si and Ge NWs have been shown in a number of studies,[31−33] while more complex morphological variations such as NW kinking often occur as a result of a change in growth direction in single crystal NWs. Such NW kinking has been controllably initiated by abrupt modification of the synthesis parameters such as pressure in a number of

Received: April 21, 2011
Revised: May 27, 2011

studies,[29,30] while it has been seen as an inherent occurrence in others.[34] For example, the Lieber research group deliberately induced acute kinking in a semiconductor wire, which coupled with alternate doping of the arms, allowed electrical probing of biological cells.[25] While extensive reports on kinking and growth defects exist for Si NWs, there is little information on similar phenomena of Ge NWs, particularly unseeded Ge NWs.

Here we present the morphological details of Ge NWs grown via an organic vapor phase based, catalyst free route.[21] Examples of, and reasoning for, lateral, longitudinal, and more complex faults seen in the NWs are presented, and an increase in their relative frequency as a function of reaction temperature and solvent is detailed. Tortuous NWs are examined and NW kinking is found to originate from interplay between NWs tending to grow along preferred crystallographic axes and NW defects being perpendicular to the NW growth direction. The study provides insight into the impact of growth direction changes and defect formation on the morphology of unseeded Ge NWs.

II. EXPERIMENTAL SECTION

Ge NWs were synthesized by thermally decomposing diphenylgermane (DPG) (>95% Gelest) in either squalene (≥98% Aldrich) or squalane (≥98% Aldrich) in custom-made quartz round bottomed flasks in a setup similar to our previously reported method.[21] In a typical synthesis, 10 mL of squalene (or squalane) was weighed out into a flask and connected to a Schlenk line via a water condenser. The setup was placed inside a three zone furnace and the system was heated to 125 °C using a 10 min ramp period under vacuum. The system was subsequently subjected to a vacuum of at least 100 mTorr for 30 min. Following this step, the system was filled with Ar and a constant flow of gas was established. The setup was ramped to reaction temperature in 15 min. As soon as the temperature had stabilized, 0.25 mL of DPG was injected via a septum cap into the organic medium at reflux. The reaction was allowed to proceed for 5 min before quenching by opening the furnace. An example of a reaction flask after the synthesis can be seen in Supporting Information Figure S1. After allowing the reaction to cool to room temperature, the products were collected in toluene via sonication for analysis. The toluene solutions were then dropcast onto lacey carbon TEM grids.

Reactions at various temperatures were analyzed. The reaction temperature used was dependent upon the solvent of choice. Squalene has a boiling point ≈395 °C, while squalane boils at ≈415 °C. As reactions were carried out in the reflux vapor of the system, reaction temperatures were carried out at temperatures above the boiling point. Lower reaction temperatures (≈400 °C) were seen to hamper NW growth. This is consistent with previous reports where Au catalysis was required to induce crystalline Ge formation at T < 400 °C.[35] We found that temperatures more than 30 °C above the respective solvent boiling point were unfavorable as they led to solvent decomposition and were thus, avoided. This meant that practically, squalene reactions could be to run at 425 °C, while squalane reactions could be run at 425 or 450 °C. The high boiling point solvents used were chosen such that the attainable temperatures allowed decomposition of the DPG. These two solvents are non-coordinating and therefore would not be expected to play an active part in influencing the crystal structure or morphology of the wire. Their only influence is to allow modulation of the reaction temperature. Increased reaction temperatures resulted in the formation of a greater amount of large diameter NWs (as evidenced by the increase in relative frequencies of type II and type III NWs). The increase in the amount of larger diameter NWs at higher temperature is consistent with the observations of Zaitseva et al. who investigated the formation of unseeded germanium nanowires in the liquid phase of high boiling point solvents.[19,21] While increased reactions temperatures were found to alter the relative percentage of each type of wire, the diameter ranges of each wire type remained constant.

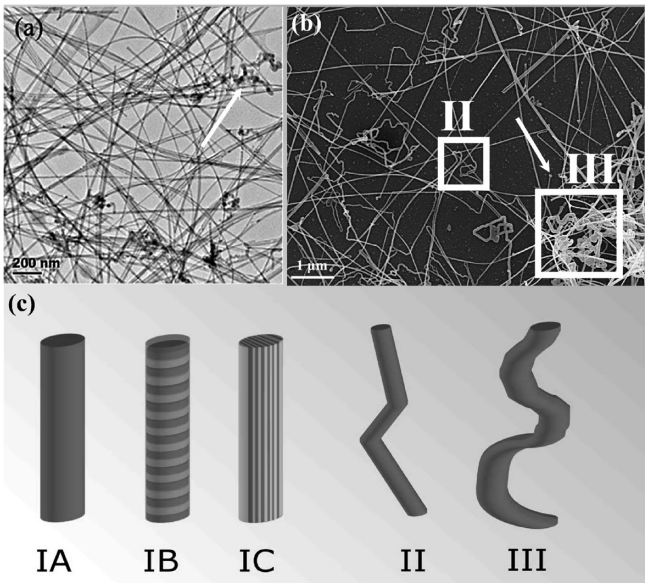

Figure 1. (a) TEM image of straight Ge NWs synthesized using squalene as the HBS. The majority of the NWs can be seen to be straight and untapered, while the arrow highlights a small area of kinked NWs. (b) SEM image of increasingly kinked NWs synthesized in squalane with specific NW types highlighted. (c) The schematic depicts the five different types of NWs discussed within the text; IA: straight, defect free NWs, IB: laterally faulted NWs, IC: longitudinally faulted NWs, II: angular NWs and III: more complex, wormlike kinked NWs.

TEM analysis was conducted using a 200 kV JEOL 2000FX microscope with a LaB_6 emission source. Additional analysis was performed using a 200 kV JEOL JEM-2100F field emission microscope. SEM analysis was performed on a Hitachi SU-70 system operating between 3 and 10 kV. Samples were prepared by dropcasting the Ge NW sample from solution onto blank Si wafers with a native oxide. X-ray diffraction (XRD) analysis was conducted by dropcasting a sample of the NWs on a zero background holder in a PANalytical X'Pert PRO MRD instrument with a Cu−K_α radiation source (λ = 1.5418 Å) and an X'celerator detector.

III. RESULTS AND DISCUSSION

Figure 1a shows a TEM image of the product of a typical squalene reaction carried out at 420 °C. The majority of the NWs were found to be straight with diameters typically between 7 and 20 nm and large aspect ratios. A small percentage of the wires (highlighted with the arrow) have larger diameter distributions and show a considerable degree of kinking. These kinked NWs were found to possess NW diameters (typically between 15 and 50 nm) which were larger than those seen in the straight NWs. The relative proportion of kinked wires to straight wires was found to significantly increase when a higher boiling point solvent was used or when the temperature was increased. Figure 1b shows an SEM image of nanowires produced from squalane (bp ≈ 420 °C) showing a greater morphological variation. A portion of these kinked NWs consisted of long (often in the order of micrometers) sections prior to very abrupt angular kinking (highlighted as area II). These NWs typically exhibited diameters between 15 and 40 nm. The remainder of the NWs were found to be extremely tortuous, "wormlike" NWs

dx.doi.org/10.1021/cg200510y |Cryst. Growth Des. XXXX, XXX, 000–000

marked III in (b) with diameters between 30 and 50 nm. Figure 1c summarizes the types of wire growth identified in a typical nonseeded synthesis. Type I are straight wires which have three subsets (only revealed in high resolution imaging (TEM)) single crystal (IA), lateral stacking faults (IB), and longitudinal stacking faults (IC). Type II is of a similar aspect ratio to type I, composed primarily of straight regions with abrupt, acute kinking and Type III is the larger aspect ratio, worm-like wires. The frequency of each wire type can be manipulated through slight modifications in the reaction temperature or changing the solvent as outlined in Table 1. The progression is such that more faulted and kinked structures are found with increasing temperature. In our case, there is also a diameter threshold above which the NW may form the more complex structural alternative (i.e., above 15 nm type II can form and above 30 nm type III can form). The following high resolution TEM and SEM study reveals the impact of growth direction changes and defects in determining the morphology for each wire type.

Table 1. Table Detailing the Relative Portions of the Different NW Types Noted in This Study

reaction solvent	reaction temperature °C	product composition
squalene	420	85% Type IA, 5% Type IB/IC, 10% Type II/III
squalane	420	60% Type IA, 10% Type IB/IC, 30% Type II/III
squalane	450	30% Type IA, 15% Type IB/IC, 55% Type II/III

Straight NW Analysis. TEM analysis of a single, defect free, type I NW is presented in Figure 2a. The NW can be seen to be a perfect, defect free, single crystal. A thin amorphous oxide coating is present at the periphery of the NW, which is consistent with all the NWs synthesized in the study. Figure 2b shows the corresponding indexed FFT from which a ⟨112⟩ growth direction was deduced. The polycrystalline electron diffraction pattern, seen in Figure 2c, was taken from a bundle of NWs and shows rings consistent with the (111), (220), and (311) type planes expected for the diamond cubic crystal structure of Ge (space group $Fd3m$ with lattice parameter a = 5.66 Å). Bulk analysis of the product was performed with powder XRD (Supporting

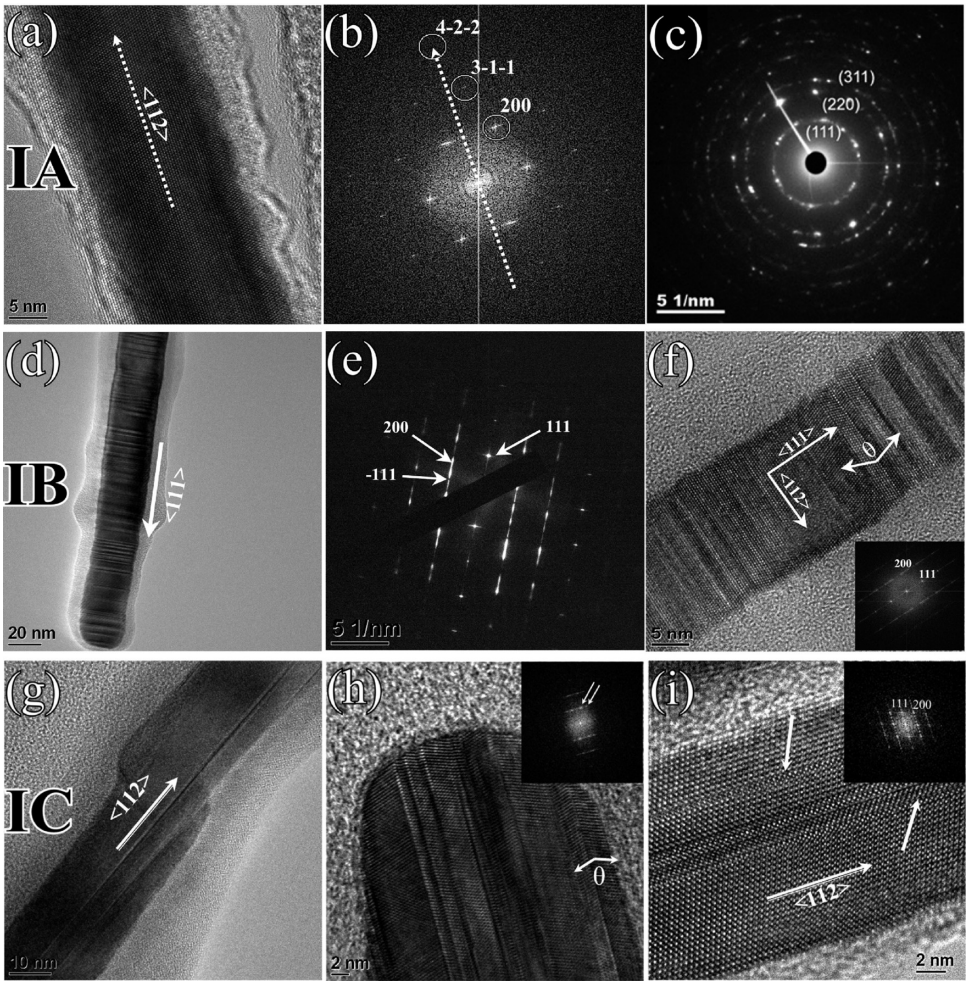

Figure 2. (a) HRTEM image of defect free NW with a ⟨112⟩ growth direction. (b) Indexed FFT used to determine the ⟨112⟩ growth direction. (c) Polycrystalline electron diffraction consistent with the presence of diamond cubic, crystalline Ge taken from a number of NWs. (d) Ge NW with lateral faults along the entire length of the NW and a ⟨111⟩ growth direction. (e) Corresponding indexed SAED pattern showing the twin defects. (f) Lattice resolved image of the faults with the marked angle equal to 141° and the FFT (inset) showing the ⟨111⟩ growth direction. (g) TEM image of longitudinally faulted NW with a ⟨112⟩ growth direction. (h) HRTEM image of a NW with faults extending to the tip with marked angle θ equal to 141° between the faults.The inset shows an FFT of the NW with arrows indicating the twinned spots. (i) HRTEM image of a NW with longitudinal faults.

dx.doi.org/10.1021/cg200510y |*Cryst. Growth Des.* XXXX, XXX, 000–000

Information Figure S2) using Cu K_α radiation. The NWs gave peaks corresponding to the (111), (220), and (311) reflections for diamond cubic Ge as expected.

In addition to the straight, defect free NWs produced by this method, straight NWs exhibiting mutually exclusive lateral (IB) and longitudinal (IC) faults were discovered to represent ≈5% of a typical squalene synthesis. The lateral defects which were evident in the type IB NWs were found to occur on the (111) plane. This indicates that lateral defects will tend to occur on NWs with a ⟨111⟩ growth direction, as indicated by the laterally faulted NW in Figure 2d. This also suggests that the reaction is not purely homogeneous in relation to growth directions as there are some thermodynamically grown, ⟨111⟩ NWs, among the kinetically grown, ⟨112⟩ NWs.[33] As indicated by the selected area diffraction (SAED) pattern in Figure 2e, the defects correspond to twin defects on the (111) plane. The streaking of the spots along [111] can be attributed to the shape effect of the thin, edge-on, twin lamellae of the regions.[32] The small (typically below 5 nm) and regular nature of the crystallographic regions, between fault twin planes more likely exerts a large influence on the morphology of the NWs. If these crystal regions were larger, this would lead to the formation of a less linear, zig-zagged NW.[36] The atomic image in Figure 2f is viewed down the $[0\bar{1}1]$ zone axis. The $[\bar{2}11]$ direction is perpendicular to the growth direction, which is parallel to the defects (and therefore lies on the (111) plane) which explains why longitudinal defects are later found on ⟨112⟩ grown wires. Similarly, if the NW was tilted 90° about the [111] axis, the $[\bar{2}11]$ zone axis would be visible and the defects would be noted running parallel to the $[0\bar{1}1]$ direction. This also agrees with the potential formation of longitudinal defects in ⟨110⟩ grown NWs.

Three different examples of type IC, longitudinally faulted NWs are presented in Figure 2. Analysis of the NWs with longitudinal defects (as shown in Figure 2g) reveals that NW growth occurs in the ⟨112⟩ direction with the defects occurring on the (111) type plane. For a NW with a ⟨112⟩ growth direction, defects on the (111) plane can exist parallel to the wire or at either a 20° or 62° angle relative to the growth direction. As a NW constrains crystal growth in two dimensions, there is a greater amount of stress compared to that in a nonconstrained crystal. The stress can be alleviated with the addition of defects. When these defects run parallel to the growth direction, there is no defect termination and the stress is minimized throughout the length of the NW. When these defects are not parallel, they continually terminate at the edge of the NW and so new defects must occur to avoid the stress returning. Therefore, defects found in the ⟨112⟩ grown, straight wires are likely to be parallel to the growth direction and thus, longitudinal. This is in good agreement with previous reports on longitudinal defect formation in Si NWs with a ⟨112⟩ growth direction.[31,32,37]

Theoretically, the formation of longitudinally faulted NWs with a ⟨110⟩ growth direction should also be possible. However, ⟨110⟩ growth is not the most favored growth in a kinetically controlled system. This has been highlighted in a previous study of Si NWs where ⟨112⟩ NW growth was shown to dominate.[33] Figure 2h shows a NW with longitudinal defects which extend to the tip of the NW. The orientation of the twin defects can be clearly seen in this image. Additionally, there are some stacking faults close to the center of the NW. The FFT inset shows a pattern which is consistent with a twin defect structure. Figure 2i is an additional example of a longitudinally faulted NW with a ⟨112⟩ growth direction. The FFT in Figure 2i indicates that there

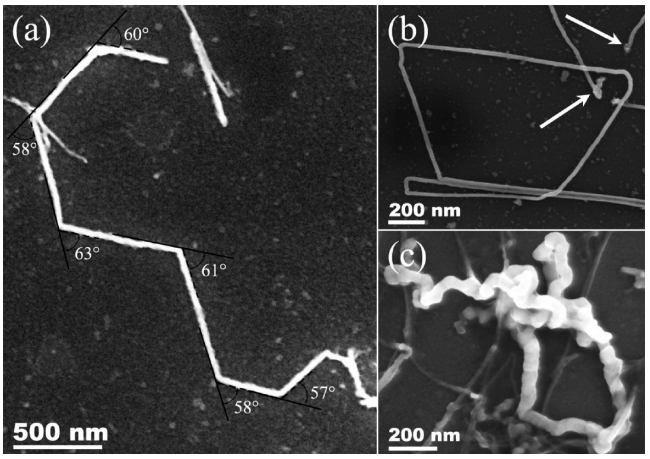

Figure 3. SEM analysis of the kinked NWs produced in squalane. (a) Type II NW showing defined ≈60° angles between growth segments. Type II (b) NW showing multiple turns along the same rotational axis. (c) Highly kinked, type III wormlike NW.

are periodic stacking faults present (marked on the image by the white arrows) as indicated by the presence of additional reflections. As the FFT suggests, the common plane containing the defects is once again the (111).

In the case of these straight NWs, it appears that faults are only present when they originate during nucleation and continue along the entire length of the NW. Faults on the {111} continue longitudinally on NWs with the ⟨112⟩ growth direction, while new faults are continually formed laterally on the {111} planes in the ⟨111⟩ grown NWs. There is no appearance of random angular faults in these type I NWs.

Kinked NW Analysis. Figure 3 shows higher magnification SEM images of complex, kinked NWs similar to those presented in Figure 1b. These wires were observed to make up a large portion of squalane syntheses (see Table 1). A type II wire is shown in Figure 3a with a defined angle of approximately 60° between each of the kinks (offset by a maximum of 3°) resulting in a regular repeating angular geometry. Figure 3b shows a further type II NW exhibiting extreme kinking, where the NW appears to be bent back on itself. This has resulted from multiple growth direction changes in similar rotational axes. NWs with denser regions on the ends of the NWs are highlighted with arrows in the image. These features, could be misconstrued as seeds, however, closer analysis reveals that these areas were actually short, kinked sections. This is further supported by TEM analysis (including tomography) (Supporting Information Figure S3). Figure 3 (c) shows a highly kinked, type III, "wormlike" NW where the extreme tortuosity has caused the various segments of the main NW to become intertwined. The type III NW presented here has a diameter ≈ 50 nm, which is consistent with other type III NWs identified throughout the course of this study.

TEM analysis allowed the deduction of how these structural features manifest themselves in terms of growth direction changes. Starting with the regular 60° kinked wires (Figure 4a), a change in growth direction from $[\bar{1}12]$ to $[\bar{2}11]$ results in an angular distortion ($\theta = 62°$). The defect marked with the dotted line, *a*, occurs at a projected 60° angle from the $[\bar{1}12]$ growth direction. At this section of the NW, the defect runs longitudinally, which makes it parallel to the [110] direction.

dx.doi.org/10.1021/cg200510y |*Cryst. Growth Des.* XXXX, XXX, 000–000

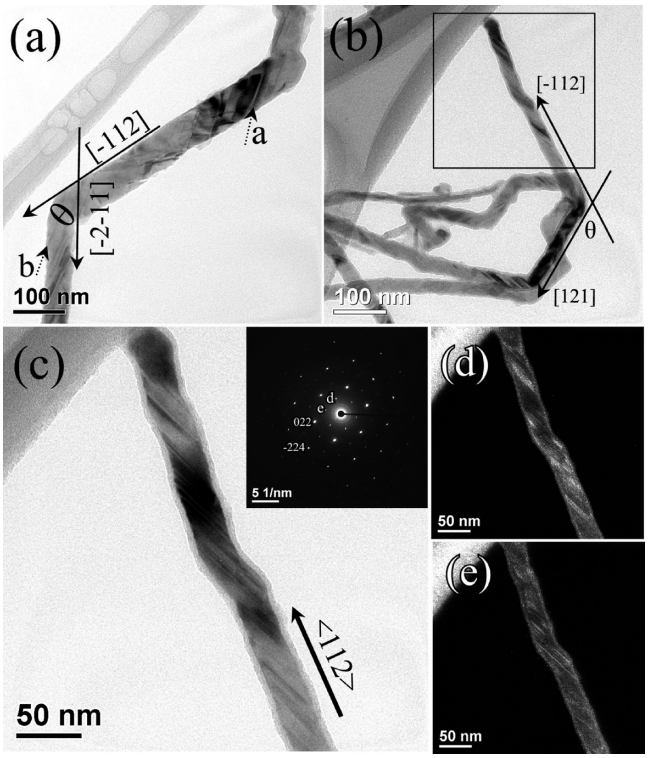

Figure 4. TEM images showing kinked NWs. (a) NW with growth direction changing from $[\bar{1}12]$ to $[\bar{2}\bar{1}1]$ with an evident angle θ of 118°. (b) Kinked NW with a characteristic 60° bend due to a change in growth direction from [121] to $[\bar{1}12]$. (c) A slightly kinked NW with the corresponding SAED (inset) taken along the $[1\bar{1}1]$ direction showing weak 1/3 type forbidden reflections: (d) and (e) are the corresponding dark field (DF)TEM images from the specific forbidden reflections marked d and e in panel (c) which highlight specific crystallographic regions.

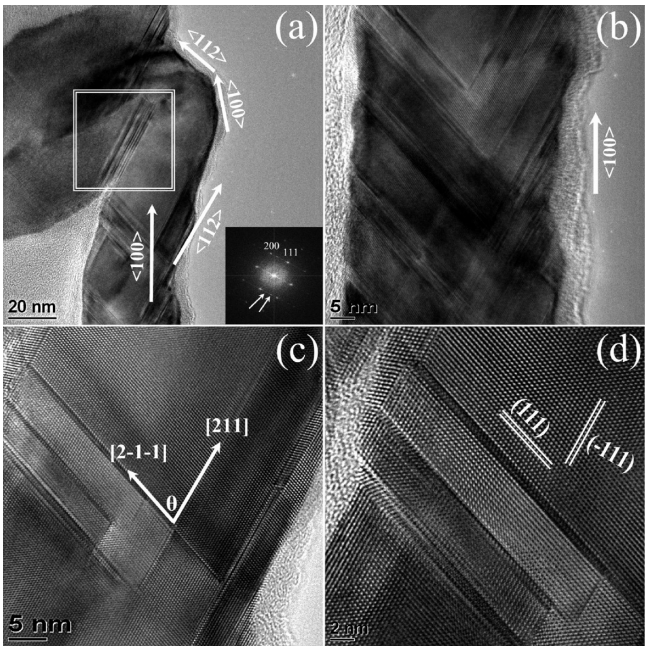

Figure 5. TEM images of a torturous "wormlike" NW with (a) faults evident even at low magnification. The inset FFT was taken from the highlighted faulted region. (b) TEM image taken further down the same NW at the ⟨100⟩ growth direction section showing additional faulting. Panels (c) and (d) are higher magnifications of the interface between the ⟨112⟩ and ⟨100⟩ growth area.

While ⟨112⟩ is a more kinetically favorable growth direction in comparison to ⟨110⟩ growth, defects which are neither parallel nor perpendicular will alleviate less stress than a longitudinal defect. This leads to interplay between the NWs growing along the preferred growth direction and faults forming longitudinally. Faults a and b are parallel to each other as they both occur on the (111) plane. The predominance of projected 60° angles seen in the defect marked b and Figure 3a indicate that NWs tend to switch from one favorable growth direction to another, rather than switching to an unfavorable growth direction. As a result, more angular defects need to form in order to continually remove the stress. Examples of these defects can be seen further in Figure 4b. The observed angles in the NW in Figure 4b can be explained by the cubic nature of Ge where the $[\bar{1}12]$ and [121] crystallographic planes have an interplanar angle of 60°. The slight discrepancy in the angle from the ideal 60° is consistent with that seen in a previous study on kinked Si NWs where a 2° offset from the ideal angle expected for such a change in growth direction was noted.[38] This deviation may be due to a small out of plane component. Similar changes in growth direction can also be used to explain the nature of the kinking encompassing long straight sections running parallel to each other as seen in Figure 3b. The abrupt 90° turn of the NW is likely due to the NW changing growth direction from the favored [112] direction to the unfavored $[1\bar{1}0]$ direction. This claim is further strengthened by the short length of this kinked region before a further right angle turn reverts growth to ⟨112⟩ re-establishing preferential growth.

Figure 4c is a higher magnification of the highlighted section of the Type II NW in Figure 4b where a more frequent occurrence of defects was investigated through the use of SAED and DFTEM. The kinked area possesses longitudinal faults, however, the short dimension of this region indicates that the favorable growth direction is the dominant factor in determining the morphology of this NW. The SAED pattern (Figure 4c, inset), taken from the kinked NW, which corresponds to the $[1\bar{1}1]$ zone axis, shows additional reflections at $1/3\{(\bar{2}24)\}$-type positions, which are related to the stacking fault content in this kinked NW. As previously noted by Gibson et al.[39] for crystalline Si, a complete diamond cubic unit cell having an AaBbCc stacking sequence, produces diffracted amplitude from each pair of layers that are phase shifted by 120°, resulting in exactly zero intensity at the 1/3 $(\bar{2}24)$-type position. However, since a real specimen may contain 3_{n+1} or 3_{n+2} layers in some areas, (i.e., a noninteger numbers of unit cells) residual intensity can sometimes be observed at the $1/3(\bar{2}24)$ position. For the Ge NWs here, the $1/3\{(\bar{2}24)\}$-type forbidden reflections present in the diffraction pattern suggests that some of the faulted lamellae have thicknesses that are 3_{n+1} or 3_{n+2} layers. In the DFTEM micrographs, which were taken from the specific reflections (Figure 4d,e), the fine brighter regions highlighted along the NW are the faulted bands corresponding to the 3_{n+1} or 3_{n+2} layers. The appearance of additional reflections is also clearly evident in the FFT and SAED patterns for the longitudinally and laterally faulted NWs presented in Figures 3 and 4, which again can be related to the stacking fault content of the NWs. The noted switching between growth directions is likely facilitated by their larger diameter relative to type I NWs. This may explain why existing research on

dx.doi.org/10.1021/cg200510y |Cryst. Growth Des. XXXX, XXX, 000–000

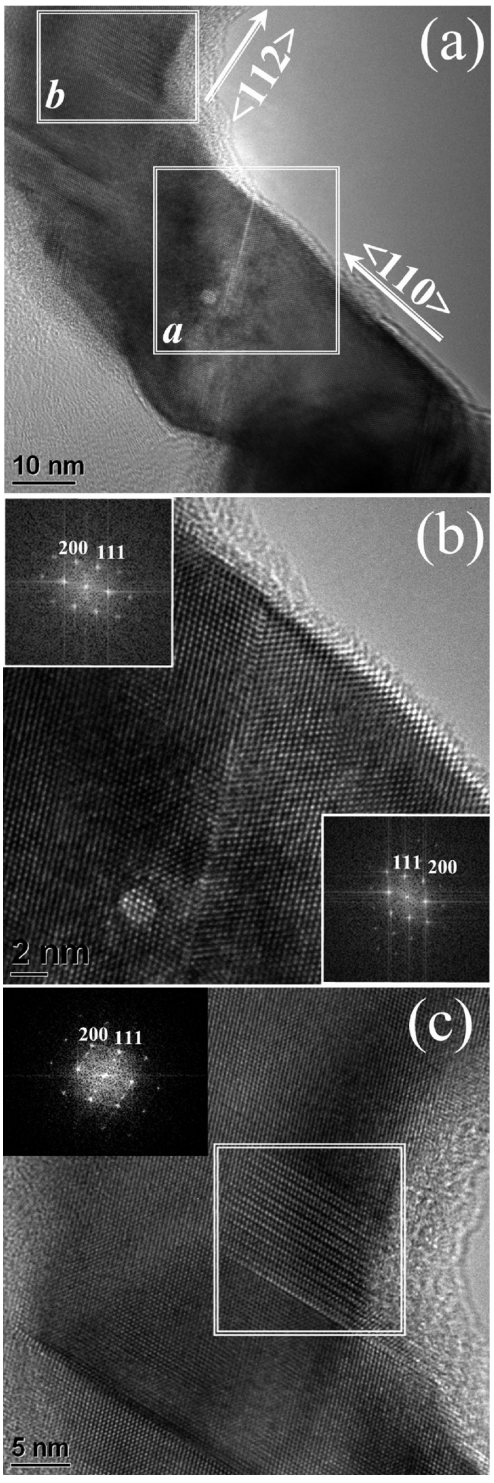

Figure 6. (a) Torturous NW with highlighted, faulted regions ***a*** and ***b*** magnified in (b) and (c) respectively. (b) High resolution image of the twinned area with FFT insets taken from either side of the fault. (c) High resolution image of the defected area with the inset FFT taken from the highlighted faulted area showing forbidden reflections as a result of stacking faults or inclined twins.

kinked NWs has largely been conducted on large diameter (≈80 nm) NWs.[25]

Type III NWs were also analyzed by HRTEM to investigate if their kinked, worm-like nature could similarly be linked to changes in NW growth direction. While it was observed that NWs with smaller diameters, typically below 35 nm, possessed primarily longitudinal or lateral faults, larger diameter NWs were found to contain more complex, atypical (not parallel or perpendicular) faulting. The existence of more complex faulting in larger diameter Si NWs has also previously been observed,[40,41] which is likely to be the case in Ge NWs. In the previous section, large angle kinks were found to be growth direction driven, while small angle kinks were defect driven. The tortuous NW shown in Figure 5a possesses a ⟨112⟩ and a ⟨100⟩ growth section; however, a higher defect density leads to the formation of a wormlike NW, the shape of which is more likely defect controlled. The highlighted section of the NW, marked in (a), consists of a ⟨112⟩ growth section, while the lower portion contains a ⟨100⟩ growth section. As the NW growth direction switches from ⟨100⟩ to ⟨112⟩, a large defect free ⟨112⟩ section is formed. This switch also results in the existing stacking faults on the {111} planes becoming longitudinal. Figure 5b,c shows two intersecting faults, one along the $[2\bar{1}\bar{1}]$ and another along the [211]. The ⟨100⟩ growth section bisects the (111) and $(\bar{1}11)$ fault planes. The angle between ⟨100⟩ and ⟨112⟩ is 35.7°, which is exactly halfway between the two sets of defects shown (marked angle θ in Figure 5c is 71.4°).

Tortuosity in NWs can occur due to different types of defects. While the example in Figure 5 showed stacking faults occurring in two different {111} planes, Figure 6 shows a type III NW growing along the ⟨110⟩ with a single defect causing a discrete angle change in the NW. A low magnification TEM image of the complex NW with two kinks evident can be seen in Figure 6 (a) with its ⟨110⟩ growth section highlighted. Again, the faulted areas (***a*** and ***b***) of interest are highlighted and further magnified in Figure 6b,c. Figure 6b shows the HR image of the twin faulted region with the indexed FFT insets taken from either side of the fault. The FFTs are both viewed down the $[01\bar{1}]$ direction; however, the switching of the (200) and the (111) indexed spots can clearly be seen. While periodic twinning has earlier been observed, like that seen in NW Figure 2f, this was absent for this NW section.

The single defect is still along the (111) plane, but differs from the earlier nanowires, with the periodic twinning, due to the defect being neither longitudinal nor lateral. The highlighted area in (c) resembles stacking faults in the region where the NW changes growth direction to ⟨112⟩. These faults appear to have periodicity similar to those seen in the longitudinally and laterally faulted NWs, and this periodicity can be seen in the FFT inset along the (111) plane between the main spots. However, as this wire is heavily tortuous, this area could equally be a region of inclined twins.[42]

IV. CONCLUSIONS

In conclusion, we have analyzed the morphological variation noted in the nonseeded synthesis of Ge NWs grown by the thermal decomposition of DPG in two HBSs. A temperature dependent increase in the degree of NW kinking was noted which was related to the stacking fault content in the NWs. The various NWs were classified into several categories. Type I were divided into three kinds of straight NWs. Type IA was defect free, Type IB possessed lateral faults and Type IC NWs contained longitudinal faults. These mutually exclusive lateral and longitudinal faults were found to be related to faulting on the (111) plane for NWs with ⟨111⟩ and ⟨112⟩ growth directions,

dx.doi.org/10.1021/cg200510y |*Cryst. Growth Des.* XXXX, XXX, 000–000

respectively. Indeed, all of the faults noted in this study occurred on the (111) plane which is the closest packed plane. Kinked and wormlike NWs were differentiated, and interplay between preferred NW growth direction and defect orientation was found to dictate the morphology of these NWs. Kinked nanowires (type II) were found to exhibit predominantly growth direction driven, large angle kinks with a small occurrence of defect driven, small angle kinks. Tortuous nanowires (Type III) were observed to have a greater occurrence of complex defect driven, small angle kinks, however, although less common, still possess some growth direction driven, large angle kinks.

■ ASSOCIATED CONTENT

Supporting Information. Example of NW growth flask post synthesis, NWs grown using oleylamine as the HBS, TEM image and video of kinked segments at the end of the NWs, image of increasingly kinked NW product formed at 450 °C. Comparison of growth directions in NWs grown using seeded and unseed approaches. Summary of the influence of diameter on preferred growth direction and faulting. This material is available free of charge via the Internet at http://pubs.acs.org.

■ AUTHOR INFORMATION

Corresponding Author
*E-mail: Kevin.M.Ryan@ul.ie.

■ ACKNOWLEDGMENT

This work was supported principally by Science Foundation Ireland (SFI) under the Principal Investigator Program under Contract No. 06/IN.1/I85 and also by the Advanced Biomimetic Materials for Solar Energy Conversion Strategic Research Cluster (Contract 07/SRC/B1160). This work was also conducted under the framework of the INSPIRE programme,funded by the Irish Government's Programme for Research in Third Level Institutions, Cycle 4, National Development Plan 2007−2013. Funding is acknowledged under the Irish Research Council for Science, Engineering and Technology (IRCSET) embark initiative for HG.

CD's and part of the TEM work were conducted under the framework of the INSPIRE programme, funded by the Irish Government's Programme for Research in Third Level Institutions, Cycle 4, National Development Plan 2007−2013.

■ REFERENCES

(1) Cao, L.; White, J. S.; Park, J.-S.; Schuller, J. A.; Clemens, B. M.; Brongersma, M. L. *Nat. Mater.* **2009**, *8*, 643–647.
(2) Kodambaka, S.; Tersoff, J.; Reuter, M. C.; Ross, F. M. *Science* **2007**, *316*, 729–732.
(3) Chan, C. K.; Zhang, X. F.; Cui, Y. *Nano Lett.* **2008**, *8*, 307–309.
(4) Tutuc, E.; Appenzeller, J.; Reuter, M. C.; Guha, S. *Nano Lett.* **2006**, *6*, 2070–2074.
(5) Garnett, E. C.; Yang, P. *J. Am. Chem. Soc.* **2008**, *130*, 9224–9225.
(6) Polyakov, B.; Daly, B.; Prikulis, J.; Lisauskas, V.; Vengalis, B.; Morris, M. A.; Holmes, J. D.; Erts, D. *Adv. Mater.* **2006**, *18*, 1812–1816.
(7) Xiang, J.; Lu, W.; Hu, Y.; Wu, Y.; Yan, H.; Lieber, C. M. *Nature* **2006**, *441*, 489–493.
(8) Nam, S.; Jiang, X.; Xiong, Q.; Ham, D.; Lieber, C. M. *Proc. Natl. Acad. Sci. U.S.A.* **2009**, *106*, 21035–21038.
(9) Wu, X.; Kulkarni, J. S.; Collins, G.; Petkov, N.; Almecija, D.; Boland, J. J.; Erts, D.; Holmes, J. D. *Chem. Mater.* **2008**, *20*, 5954–5967.
(10) Wu, Y.; Fan, R.; Yang, P. *Nano Lett.* **2002**, *2*, 83–86.
(11) Zakharov, N. D.; Werner, P.; Gerth, G.; Schubert, L.; Sokolov, L.; Gösele, U. *J. Cryst. Growth* **2006**, *290*, 6–10.
(12) Adhikari, H.; Marshall, A. F.; Chidsey, C. E. D.; McIntyre, P. C. *Nano Lett.* **2006**, *6*, 318–323.
(13) Heitsch, A. T.; Fanfair, D. D.; Tuan, H. Y.; Korgel, B. A. *J. Am. Chem. Soc.* **2008**, *130*, 5436–5437.
(14) Hanrath, T.; Korgel, B. A. *J. Am. Chem. Soc.* **2002**, *124*, 1424–1429.
(15) Wang, D. W.; Dai, H. J. *Angew. Chem.-Int. Ed.* **2002**, *41*, 4783–4786.
(16) Barrett, C. A.; Gunning, R. D.; Hantschel, T.; Arstila, K.; O'Sullivan, C.; Geaney, H.; Ryan, K. M. *J. Mat. Chem.* **2010**, *20*, 135 144.
(17) Tuan, H.-Y.; Lee, D. C.; Hanrath, T.; Korgel, B. A. *Chem. Mater.* **2005**, *17*, 5705–5711.
(18) Ge, M.; Liu, J. F.; Wu, H.; Yao, C.; Zeng, Y.; Fu, Z. D.; Zhang, S. L.; Jiang, J. Z. *J. Phys. Chem. C* **2007**, *111*, 11157–11160.
(19) Zaitseva, N.; Harper, J.; Gerion, D.; Saw, C. *Appl. Phys. Lett.* **2005**, *86*, 053105–053105−3.
(20) Hobbs, R. G.; Barth, S.; Petkov, N.; Zirngast, M.; Marschner, C.; Morris, M. A.; Holmes, J. D. *J. Am. Chem. Soc.* **2010**, *132*, 13742–13749.
(21) Barrett, C. A.; Geaney, H.; Gunning, R. D.; Laffir, F. R.; Ryan, K. M. *Chem. Commun.* **2011**, *47*, 3843–3845.
(22) He, R.; Gao, D.; Fan, R.; Hochbaum, A.; Carraro, C.; Maboudian, R.; Yang, P. *Adv. Mater.* **2005**, *17*, 2098–2102.
(23) Chen, H. A.; Wang, H.; Zhang, X. H.; Lee, C. S.; Lee, S. T. *Nano Lett.*, *10*, 864-868.
(24) Holmes, J. D.; Johnston, K. P.; Doty, R. C.; Korgel, B. A. *Science* **2000**, *287*, 1471–1473.
(25) Tian, B. Z.; Xie, P.; Kempa, T. J.; Bell, D. C.; Lieber, C. M. *Nat. Nanotechnol.* **2009**, *4*, 824–829.
(26) Schmidt, V.; Senz, S.; GÃsele, U. *Nano Lett.* **2005**, *5*, 931–935.
(27) Hanrath, T.; Korgel, B. A. *Small* **2005**, *1*, 717–721.
(28) Wu, Y.; Yang, P. *Chem. Mater.* **2000**, *12*, 605–607.
(29) Madras, P.; Dailey, E.; Drucker, J. *Nano Lett.* **2009**, *9*, 3826–3830.
(30) Lugstein, A.; Steinmair, M.; Hyun, Y. J.; Hauer, G.; Pongratz, P.; Bertagnolli, E. *Nano Lett.* **2008**, *8*, 2310–2314.
(31) Davidson, F. M.; Lee, D. C.; Fanfair, D. D.; Korgel, B. A. *J. Phys. Chem. C* **2007**, *111*, 2929–2935.
(32) Wang, Z. W.; Li, Z. Y. *Nano Lett.* **2009**, *9*, 1467–1471.
(33) Su, Z. X.; Dickinson, C.; Wan, Y. T.; Wang, Z. L.; Wang, Y. W.; Sha, J. A.; Zhou, W. Z. *CrystEngComm* **2010**, *12*, 2793–2798.
(34) Kang, K.; Gu, G. H.; Kim, D. A.; Park, C. G.; Jo, M.-H. *Chem. Mater.* **2008**, *20*, 6577–6579.
(35) Chockla, A. M.; Korgel, B. A. *J. Mat. Chem.* **2009**, *19*, 996–1001.
(36) Caroff, P.; Dick, K. A.; Johansson, J.; Messing, M. E.; Deppert, K.; Samuelson, L. *Nature Nanotechnol.* **2009**, *4*, 50–55.
(37) Wittemann, J. V.; Munchgesang, W.; Senz, S.; Schmidt, V. *J. Appl. Phys* **2010**, *107*, No. 096105.
(38) Hyun, Y. J.; Lugstein, A.; Steinmair, M.; Bertagnolli, E.; Pongratz, P. *Nanotechnology* **2009**, *20*, 5.
(39) Gibson, J. M.; Lanzerotti, M. Y.; Elser, V. *Appl. Phys. Lett.* **1989**, *55*, 1394–1396.
(40) Akhtar, S.; Usami, K.; Tsuchiya, Y.; Mizuta, H.; Oda, S. In *Microprocesses and Nanotechnology, 2007 Digest of Papers*; IEEE: New York, 2007, pp 536−537.
(41) Akhtar, S.; Usami, K.; Tsuchiya, Y.; Mizuta, H.; Oda, S. *Jpn. J. Appl. Phys.* **2008**, *47*, 5053–5056.
(42) Dahmen, U.; Hetherington, C. J. D.; Radmilovic, V.; Johnson, E.; Xiao, S. Q.; Luo, C. P. *Microsc. Microanal.* **2002**, *8*, 247–256.